



Power-law tail in lag time distribution underlies bacterial persistence

Emrah Şimşek^a and Minsu Kim^{a,b,c,1}

^aDepartment of Physics, Emory University, Atlanta, GA 30322; ^bGraduate Division of Biological and Biomedical Sciences, Emory University, Atlanta, GA 30322; and ^cEmory Antibiotic Resistance Center, Emory University, Atlanta, GA 30322

Edited by Lalita Ramakrishnan, University of Cambridge, Cambridge, United Kingdom, and approved July 29, 2019 (received for review March 5, 2019)

Genetically identical microbial cells respond to stress heterogeneously, and this phenotypic heterogeneity contributes to population survival. Quantitative analysis of phenotypic heterogeneity can reveal dynamic features of stochastic mechanisms that generate heterogeneity. Additionally, it can enable a priori prediction of population dynamics, elucidating microbial survival strategies. Here, we quantitatively analyzed the persistence of an *Escherichia coli* population. When a population is confronted with antibiotics, a majority of cells is killed but a subpopulation called persisters survives the treatment. Previous studies have found that persisters survive antibiotic treatment by maintaining a long period of lag phase. When we quantified the lag time distribution of *E. coli* cells in a large dynamic range, we found that normal cells rejuvenated with a lag time distribution that is well captured by an exponential decay $\exp(-kt)$, agreeing with previous studies. This exponential decay indicates that their rejuvenation is governed by a single rate constant kinetics (i.e., k is constant). Interestingly, the lag time distribution of persisters exhibited a long tail captured by a power-law decay. Using a simple quantitative argument, we demonstrated that this power-law decay can be explained by a wide variation of the rate constant k . Additionally, by developing a mathematical model based on this biphasic lag time distribution, we quantitatively explained the complex population dynamics of persistence without any ad hoc parameters. The quantitative features of persistence demonstrated in our work shed insights into molecular mechanisms of persistence and advance our knowledge of how a microbial population evades antibiotic treatment.

persister | persistence | lag time | power-law decay | phenotypic heterogeneity

Many stochastic systems, although they may consist of completely different microscopic components, can exhibit quantitatively similar fluctuations, which suggests the universality in stochastic processes. For example, a wide variety of seemingly unrelated stochastic processes, e.g., radioactive decay, the number of car accidents at a given site, etc., can be captured by the Poisson dynamics, thus sharing similar features, e.g., exponential time distribution of the events (1, 2). Importantly, demonstrating such quantitative features can provide an understanding of dynamic mechanisms that generate system-level fluctuations, enabling a priori prediction of fluctuations. Furthermore, demonstrating such quantitative features can reveal connections between seemingly unrelated phenomena that share similar features.

A microbial cell is a stochastic system because biochemical reactions inside of it are inherently stochastic (3–9). Due to this inherent stochasticity, genetically identical cells can exhibit a great deal of phenotypic heterogeneity (10–14). From a clinical perspective, the most important example of phenotypic heterogeneity is a phenomenon known as persistence (15–17). As first reported by Joseph Bigger (18), when a clonal bacterial population is exposed to a bactericidal drug, a majority of cells die quickly while a minority called persisters survive for long periods of time, resulting in complex population survival dynamics.

To better understand these population dynamics, extensive studies have focused on molecular mechanisms of persistence.

While a large number of genes that can alter the levels of persistence have been identified, there is a substantial controversy regarding how these genes are activated and how they contribute to persistence (19–24). As such, with the current knowledge of molecular mechanisms alone, we cannot predict the population dynamics of persistence, e.g., what percentage of cells in a population is persisters and how their percentage changes over time.

Various theoretical modeling efforts have been made to understand the population dynamics of persistence (25–29). These models typically contain coupled differential equations with parameters describing the dynamics of antibiotic killing and switching between normal and persister cells. To explain the complexity of population dynamics of persistence, some models introduced additional processes, e.g., 2 different types of persisters or dependence of switching on substrate/antibiotic concentrations, etc. The parameter values associated with these processes were often determined by fitting the models to population dynamics data. However, the number of free parameters in some of these models raises concerns about overfitting. More importantly, the quantitative signature governing persistence has rarely been discussed in these studies.

Single-cell resolution imaging was proven to be a valuable tool for studying persistence. It was shown that when cells in stationary phase (hence nondividing) were suspended in a fresh growth-permissive medium, a majority of cells rejuvenate and resume growth immediately, but a small subpopulation maintains the nondividing state (i.e., lag phase) for an extended period of time (25, 30–32). Because a nondividing state confers cells tolerance to antibiotics, this subpopulation can survive antibiotic treatment, contributing to persistence. Collectively, these studies

Significance

Persisters are antibiotic-tolerant cells that can evade antibiotic killing by maintaining long lag phase. They complicate antibiotic treatment, leading to treatment failure. Extensive studies in the field found that a myriad of molecular mechanisms leads to persisters. However, we still do not quantitatively understand, nor can we predict, the population dynamics of persistence, e.g., how the number of persisters changes over time. To address this issue, we characterized the lag time distribution of persisters. We observed a power-law decay in the tail of the distribution. We showed that this feature can quantitatively account for the population dynamics of persistence without ad hoc parameters. Additionally, we showed how this simple quantitative feature can emerge due to complicated molecular mechanisms.

Author contributions: E.Ş. and M.K. designed research; E.Ş. performed research; E.Ş. contributed new reagents/analytic tools; E.Ş. and M.K. analyzed data; and E.Ş. and M.K. wrote the paper.

The authors declare no conflict of interest.

This article is a PNAS Direct Submission.

Published under the PNAS license.

¹To whom correspondence may be addressed. Email: minsu.kim@emory.edu.

This article contains supporting information online at www.pnas.org/lookup/suppl/doi:10.1073/pnas.1903836116/-DCSupplemental.

established that long lag phase plays a critical role in persistence. However, a quantitative study of long lag phase is challenging, due to very low levels of cells with long lag phase. For example, although some studies directly observed these cells using single-cell microscopy, due to low sample size, it was difficult to quantitatively analyze their lag time (25, 32, 33). Although other methods were used to deduce the long lag time of persisters, e.g., by measuring microcolony appearance dynamics (ScanLag) (33) or fluorescence dilution (34), these are indirect measurements.

In this work, we directly monitored a large number of wild-type *Escherichia coli* cells using single-cell microscopy and quantitatively characterized a large dynamic range of their lag time distribution, demonstrating its intricate quantitative feature. Additionally, we show that this quantitative feature alone can account for the population dynamics of persistence without ad hoc parameters. We then discuss the population structure that gives rise to the observed quantitative feature, the possible connections between this quantitative feature and the current molecular understanding of persistence, and the clinical implication of this quantitative feature.

Results and Discussion

Multiphase Population Dynamics of Isogenic Bacteria Exposed to an Antibiotic. We first characterized the population dynamics of persistence by measuring a time-dependent killing curve of a population exposed to an antibiotic. The stationary phase was shown to play an important role in persister generation; for example, maintaining a culture in the exponential phase for an extended period of time eliminates persisters (16). Thus, to enrich persisters in a culture, most studies kept cells in stationary phase before suspending them in fresh medium containing an antibiotic (25, 30, 31, 34, 35). In our experiments, we kept cells in stationary phase for 3 d and suspended them in fresh LB medium containing ampicillin (100 $\mu\text{g}/\text{mL}$); the moment of suspension defines time 0. To measure a time-dependent killing curve, we performed a colony-forming unit (CFU) assay at different times by spreading a small volume of the culture onto an LB agar plate containing no ampicillin. We then incubated the plates overnight, enumerated CFUs, and determined N_{CFU} (the number of CFUs at time t normalized by the number of CFUs at time 0). Agreeing with previous studies, a complex multiphase killing curve was observed (Fig. 1) (25, 36–38). Importantly, the long tail of the curve indicates persistence.

Single-Cell-Level Observation of Lag Time. Previous studies have shown that a long lag phase of a minority of cells contributes to persistence (25, 30, 31). Thus, we used single-cell time-lapse microscopy to determine the periods of lag phase (lag time) of individual cells. We prepared a culture as described above and determined how long it takes for cells from a stationary-phase culture to rejuvenate and resume growth in fresh LB medium. Fig. 2A shows a rejuvenation probability distribution, which is also called a lag time distribution in the field (these 2 terms are used interchangeably in this article). The rejuvenation probability decreased rapidly in the first 100 min, and this decrease was well approximated by an exponential decay (linear line in green shaded region in Fig. 2A). This exponential decay agrees with previous observations in other studies (SI Appendix, Fig. S1).

What distinguishes our dataset from others is its large dynamic range. The aforementioned studies of lag time distribution characterized 2 or 3 orders of magnitude of decrease in the distribution, thus focusing mostly on rejuvenation of normal cells. Although recent studies directly observed a minority of cells with a long lag phase (i.e., persisters) with single-cell microscopy, due to low sample size, it was difficult to precisely quantify or analyze their rejuvenation probability (25, 32, 33). In this work, by tracking a large number of cells ($\sim 12,800$ cells in 3 independent experiments), we quantified a large dynamic range of the rejuvenation probability. We observed that after the initial exponential decay of rejuvenation probability (by nearly 3 orders of

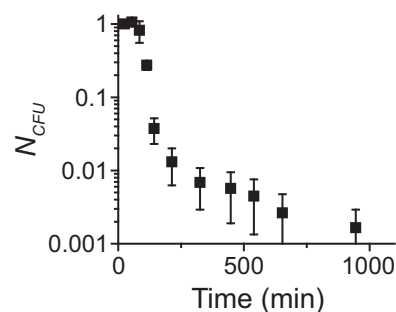


Fig. 1. Time-dependent killing curve of a population exposed to ampicillin. Stationary-phase cells were suspended in fresh LB medium containing 100 $\mu\text{g}/\text{mL}$ ampicillin (time 0). A colony-forming unit (CFU) assay was performed at different times. N_{CFU} represents normalized CFU, i.e., the number of CFUs at time t divided by the number of CFUs at time 0. Agreeing with previous studies (25, 36, 37), a complex multiphase killing curve was observed. The long tail of the curve indicates persistence. We performed additional experiments to confirm that this tail is not due to mutation (see SI Appendix, Fig. S3 for details). For each time point t , at least 2 biological replicates were performed, and their mean (data points) and SD (error bars) were shown. Within each biological replicate, at least 4 technical replicates were performed, and their average was used for the plot.

magnitude), the decrease slows down dramatically, deviating from the exponential decay (to the right of the green shaded region in Fig. 2A). Interestingly, when we replotted the data in the second regime in a log-log scale, we observed a linear decrease (Fig. 2A, Inset), suggesting a power-law decay. In many statistical studies, it is common to use logarithmic data binning to show a power-law decay of a distribution (39). When we binned our data logarithmically, we again observed the same linear trend (Fig. 2B); note that the values of all our raw data as well as processed data (logarithmically binned) are provided in SI Appendix. The power-law exponent was found to be approximately -2 (Fig. 2B, line). Power-law distribution is a widespread feature in many stochastic processes, observed in physics, ecology, earth sciences, and social sciences (e.g., self-organized criticality, earthquake, word usage, etc.) (39). Typically, these empirical distributions exhibit a power-law decay only in the tail; it is rare that distributions follow a power-law decay for all their values. This is the case for the rejuvenation probability observed in our study as well.

Collectively, our single-cell-level data above indicate that the rejuvenation probability $f(\tau)$ is biphasic and well captured by the following:

$$f(\tau) = \begin{cases} A_1 \cdot \exp(-k \cdot \tau) & \text{for } \tau < \tau_0 \\ A_2 \cdot \tau^{-\beta} & \text{for } \tau \geq \tau_0 \end{cases}, \quad [1]$$

where k , τ_0 , and β are the rate constant in the initial exponential decay, the time at which the probability distribution transitions to a power-law decay, and the power-law exponent, respectively. A_1 and A_2 are normalization constants that are related to the proportion of normal and persister cells. The values of these parameters were determined from the experimental data as described in SI Appendix, Supplementary Method and provided in Fig. 2 and SI Appendix, Table S1.

Time Delay of Ampicillin Killing. Having quantitatively characterized the temporal distribution of rejuvenation probability, we sought to use this distribution to better understand the complex time-dependent killing curve (Fig. 1). Importantly, persisters are different from antibiotic-resistant cells in that once persisters rejuvenate and resume growth, they are killed by antibiotics. Therefore, to understand the time-dependent killing curve, we must know how quickly growing cells are killed by ampicillin. Propidium iodide (PI) staining was previously shown to be an

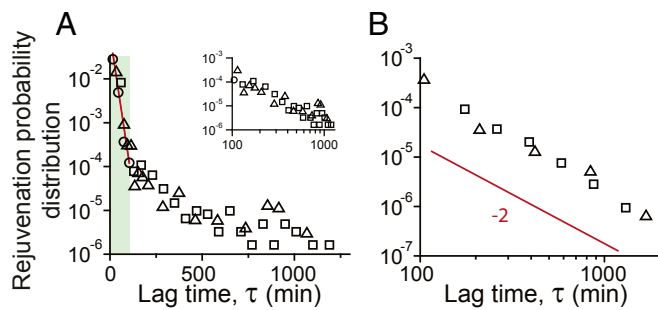


Fig. 2. Rejuvenation probability distribution (or lag time distribution). (A) Using time-lapse microscopy, we determined the time points at which cells from stationary phase rejuvenate and resume growth upon suspension to fresh LB medium (~12,800 cells were analyzed in 3 independent experiments). The rejuvenation probability initially decreased rapidly over time (green region), and this initial decrease was well approximated by an exponential decay (linear line). After a rapid decrease of nearly 3 orders of magnitude, the decrease slows down dramatically, deviating from the exponential decay (to the right of the green shaded region). In the *Inset*, we replotted this late regime in a log-log scale. A linear decrease in a log-log scale suggests a power-law decay. Three different symbols represent the data obtained from 3 independent experiments. (B) In statistical studies, it is common to use logarithmic data binning to visualize a power-law decay of a distribution (39). The data shown in the *Inset* (Fig. 2A) were replotted after logarithmic binning. The power-law exponent is approximately -2 (the red line has a slope of -2). Note that the values of all our raw data as well as processed data (logarithmically binned) are provided in *SI Appendix*. Additionally, we performed more experiments to confirm that the initial cell density has little effect on our observation (see *SI Appendix, Fig. S4* for details). The biphasic decay plotted here was mathematically formulated as $f(\tau)$ in Eq. 1. The parameter values in Eq. 1 were determined using the experimental data as described in *SI Appendix, Supplementary Method* ($\tau_0 = 93$ min, $k = 0.063$ min $^{-1}$, and $\beta = -2.1$, $A_1 = 0.0622$ min $^{-1}$, and $A_2 = 2.42$ min $^{-1}$).

excellent indicator of dead *E. coli* cells (40–44). We additionally confirmed that PI is a good indicator for cell death by ampicillin; when we incubated cells with ampicillin and PI for 80 min and spread them on an LB agar plate containing no ampicillin, none of the PI stained (PI+) cells grew (see *SI Appendix, Supplementary Method* for detail). One issue of PI is the loss of nucleic acids upon lysis by ampicillin. PI stains nucleic acids, but lysis results in the loss of cytoplasmic contents, including nucleic acids (40–44). Hence, lysed cells are, although they are clearly dead, not stained by PI. On the other hand, we can distinguish these lysed cells by their refractivity; when observed via phase-contrast microscopy, a live *E. coli* cell is normally refractive (i.e., it exhibits a dark area with sharp boundaries), whereas lysed cells exhibit poor phase contrast with diffuse boundaries (44). Therefore, we tracked both PI staining and lysis to evaluate ampicillin killing. We found that on average it takes 102 min for ampicillin to kill growing cells (*SI Appendix, Fig. S2*). We denote this time delay of killing by Δ (=102 min). A similar time delay of ampicillin killing was observed in previous studies (45).

Mathematical Framework Bridging Lag Time Distribution and Time-Dependent Killing Curve. To quantitatively understand the population dynamics of persistence, one could model switching between normal and persister cells using ordinary differential equations. More realistic models can be constructed by including the dependence of switching rates on various factors such as substrate concentration (e.g., see ref. 28). One potential problem of this approach, however, is overfitting; although a model may fit a curve, fitting itself may not justify the underlying assumption of the model. Here, we take an alternative approach. We believe that our single-cell studies above have identified the central kinetics underlying persistence (i.e., the biphasic decay of rejuvenation probability distribution). If these kinetics govern

persistence as we believe, they must be able to account for the time-dependent killing curve without any ad hoc parameters.

To do so, we must clarify the relationship between rejuvenation probability and a time-dependent killing curve. As discussed above, a time-dependent killing curve is measured by performing CFU assays at different times, that is, a small volume of a sample was taken from a culture growing in LB with ampicillin and spread on an LB plate (without ampicillin) at time t . Thus, the CFU data report the number of viable cells at the time t . Given the time delay of ampicillin killing Δ (as shown above), the cells that had rejuvenated and resumed growth at any time before $t - \Delta$ would be killed, failing to form colonies. Mathematically put, the fraction of dead cells at time t is then equal to $\int_0^{t-\Delta} f(\tau) d\tau$, where $f(\tau)$ is the rejuvenation probability. Conversely, the fraction of viable cells capable of forming colonies on an LB plate when assayed at time t , $g(t)$, is given by the following:

$$g(t) = 1 - \int_0^{t-\Delta} f(\tau) d\tau. \quad [2]$$

Because we already know the function of rejuvenation probability $f(\tau)$ (Eq. 1), we can calculate $g(t)$. The result was plotted as a black curve in Fig. 3. In the same figure, we replotted the empirical time-dependent killing curve (from Fig. 1) as black points, which shows a good agreement. Importantly, our mathematical model highlights 3 different phases. First, for t less than Δ (=102 min), there would not be enough time for ampicillin to kill cells. Thus, $g(t)$ is 1 (green region in Fig. 3). A majority of cells rejuvenate and resume growth within the first 93 min (Fig. 2), but these cells are killed by ampicillin after a time delay Δ , leading to a rapid decay of N_{CFU} between Δ (=102 min) and Δ (=102) + 93 min (red region in Fig. 3). The rejuvenation probability exhibits a long tail after 93 min (Fig. 2B), leading to a long stretch of N_{CFU} after Δ (=102) + 93 min (blue region in Fig. 3). Thus, the rejuvenation probability can account for the complex time-dependent killing curve without ad hoc parameters.

Here, all of the parameter values in this model were determined empirically from single-cell-level experiments (Fig. 2) and thus would be affected by experimental error. Next, by allowing the

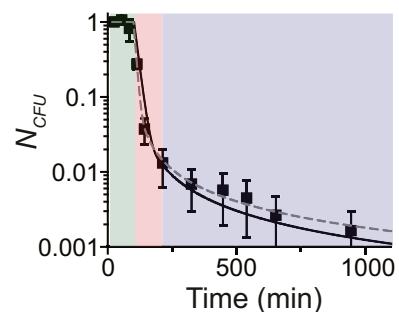


Fig. 3. Comparing the model prediction of a time-dependent killing curve with experimental data. We mathematically related the rejuvenation probability distribution (f) and the fraction of viable cells (g) in Eq. 2. Using the rejuvenation distribution f (which was fully specified in Eq. 1 and Fig. 2), we calculated the fraction of viable cells g and plotted the result as a black curve. The empirical time-dependent killing curve (from Fig. 1) was replotted as black points, which show a good agreement. Importantly, our mathematical model highlights 3 different phases as marked by different shades. See text for details. Here, the parameter values used to compute g were previously obtained using the data plotted in Fig. 2. We then varied these parameter values to find the best fit. The best-fit curve (gray dashed curve) looked similar to the original prediction based on empirically determined parameters (black solid curve). Also, the best-fit parameter values are similar to those determined empirically (*SI Appendix, Table S1*).

parameter values to vary, we searched for the best fit of the model to the killing curve. The best-fit curve (gray dashed curve in Fig. 3) agreed with the experimental killing data (black points) marginally better than the original prediction (black solid curve), although they are very similar. The parameter values from the fitting are found to be similar to those used originally (determined empirically from single-cell-level data) (*SI Appendix, Table S1*).

Quantitative Mechanisms for Exponential or Power-Law Decays in Rejuvenation Probability. An exponential decay distribution is common in natural phenomena [e.g., radioactive decay (2)]. An exponential decay indicates first-order kinetics with a single rate constant. To demonstrate this point, we consider nongrowing cells rejuvenating and resuming growth at a constant rate of k . Then, the number of nongrowing cells at a given time $N(\tau)$ is governed by the following:

$$\frac{dN(\tau)}{d\tau} = -kN(\tau). \quad [3]$$

The solution of Eq. 3 is as follows:

$$N(\tau) \propto \exp(-k \cdot \tau). \quad [4]$$

The rejuvenation probability we measured in our experiments refers to the number of cells resuming their growth during a given time interval $\Delta\tau$, $\bar{N}(\tau)$, which is given mathematically by the following:

$$\bar{N}(\tau) = -\frac{\Delta N(\tau)}{\Delta\tau} \propto k \cdot \exp(-k \cdot \tau). \quad [5]$$

Eq. 5 indicates that a homogeneous population that resumes growth with a single rejuvenation constant k exhibits an exponential decay in rejuvenation probability distribution.

How can we understand the power-law decay in the later part of the distribution (Fig. 2B)? The mathematical derivation shown above (Eqs. 3–5) clearly indicates that a homogeneous population with a single rejuvenation constant cannot exhibit a power-law decay. To quantitatively understand a power-law decay, we then consider a heterogeneous population. For the sake of simplicity, we first consider a population consisting of 2 subpopulations with 2 different rejuvenation constants k_1 and k_2 . In this case, using Eq. 5, we can write that the number of cells resuming their growth at a specific time τ , $\bar{N}(\tau)$, is given by the following:

$$\bar{N}(\tau) \propto k_1 \cdot \exp(-k_1 \cdot \tau) + k_2 \cdot \exp(-k_2 \cdot \tau). \quad [6]$$

Extending this formula, for a large number of such subpopulations, we have the following:

$$\bar{N}(\tau) \propto \sum_{i=1}^n k_i \cdot \exp(-k_i \cdot \tau), \quad [7]$$

or

$$\bar{N}(\tau) \propto \int_0^{\infty} k \cdot \exp(-\tau \cdot k) \cdot dk. \quad [8]$$

Since $\int_0^{\infty} k \cdot \exp(-\tau \cdot k) \cdot dk = -(d/d\tau) \int_0^{\infty} \exp(-\tau \cdot k) \cdot dk$ and $\int_0^{\infty} \exp(-\tau \cdot k) \cdot dk = 1/\tau$, Eq. 8 becomes the following:

$$\bar{N}(\tau) \propto \frac{1}{\tau^2}. \quad [9]$$

Thus, for a heterogeneous population in which cells rejuvenate with various rate constants, the rejuvenation probability is expected to exhibit a power-law decay with exponent of -2 , as we observed in our experiments (Fig. 2B). Please note that we further extended this argument in *SI Appendix*. Above, the integral

over k has an infinite upper-hand limit (Eq. 8), which implies that the population size is infinite. By considering an integral with finite limits, we showed that the finite population size sets the temporal bound for which the power-law holds (*SI Appendix, Supplementary Note 1*). In addition, above we assumed a uniform distribution of k to provide an intuitive explanation of the power-law decay with the exponent of -2 . By introducing a weighting function of k , we showed that this assumption is not critical to explaining the observed power-law decay (*SI Appendix, Supplementary Note 2*).

Power-Law Decay Can Provide a Quantitative Framework for Understanding Complex Molecular Processes Underlying Persistence.

How can we relate this power-law nature of rejuvenation probability distribution to the current molecular understanding of persistence? Molecular mechanisms of persistence have been extensively characterized (16, 46, 47). Previous studies of persisters have shown that toxin and antitoxin systems cause persistence (25, 48–51), but increasing evidence supports that there are many other genes that lead to persistence, such as *phoU*, *tolC*, *oxyR*, etc. (52–55). Additionally, various errors in the cell replication cycle or metabolism as well as cells' stress response to such errors lead to the nondividing state of persisters (56–62). Collectively, these studies indicate that a myriad of different molecular processes can contribute to generation and rejuvenation of persisters. For example, some cells could enter a nondividing state because of toxin overproduction and rejuvenate when toxins get degraded (by antitoxins). Some cells could enter a nondividing state due to glitches in DNA replication and rejuvenate when the glitches are repaired. As such, a persister subpopulation is a diverse collection of various cells whose growth was transiently halted by different mechanisms (63). Since different persister cells can enter and exit a lag phase through different mechanisms, rejuvenation kinetics of persisters are expected to be highly heterogeneous, meaning a wide variation of rejuvenation constants within a persister subpopulation. As our derivation above (Eqs. 6–9) shows, such a wide variation of rejuvenation constants would lead to a power-law decay in rejuvenation probability. Therefore, our findings of a power-law decay in rejuvenation probability distribution agree with previous findings that a myriad of mechanisms generate persisters. However, we emphasize that this connection between the molecular mechanisms and power-law decay distribution is speculative, and more studies are needed to establish this connection.

Further Implication of a Power-Law Decay. In statistics and probability, a long tail in a probability distribution indicates a large number of occurrences far from the central part of the distribution. A power-law distribution is a classic example of a long-tailed distribution. This is why a power-law decay in rejuvenation probability distribution leads to a long stretch in the time-dependent killing curve (Fig. 3). In fact, we quantitatively explained this stretch with the power-law distribution without invoking any ad hoc parameters (Fig. 3).

From a clinical point of view, this long tail distribution is problematic because it indicates that some persister cells rejuvenate and resume growth after maintaining a very long period of lag phase. Unfortunately, many conventional antibiotics have little efficacy for these cells during lag phase, killing them only once they rejuvenate. Therefore, for infections containing persister cells, an extended antibiotic treatment is required for eradication. This is why for infections by agents with a high number of persisters, e.g., *Mycobacterium tuberculosis*, antibiotic treatment lasts more than 6 mo (still then, the chance of eradication is not 100%). Therefore, our observation of a power-law decay in rejuvenation probability further highlights the need to develop new interventions to rejuvenate persister cells [as was previously demonstrated (64)] or new antibiotics that can directly

target persister cells (65). Importantly, persistence is a general phenomenon as it has been observed not only for bacteria but also for fungi and mammalian cells (66–68). It would be interesting to investigate the generality of our findings.

Methods

Strain and Cell Culture. We used an *E. coli* K12 NCM3722 Δ motA strain (69). For batch cultures, cells were cultured at 37 °C with shaking at 250 rpm in a water bath (New Brunswick Scientific). To monitor growth in batch cultures, the optical density (OD₆₀₀) of the culture was measured using a Genesys20 spectrophotometer (Thermo Fisher) with a standard cuvette (16.100-Q-10/Z8.5; Starna Cells). Our typical experimental procedure was as follows. Cells were taken from –80 °C stocks and first cultured in an LB medium for 4 to 6 h (seed culture). Then, they were transferred to N[–]C[–] minimal medium (pH = 7) (70) supplemented with 40 mM ammonium chloride and 40 mM glucose (glucose minimal medium) at very low densities (typically lower than OD₆₀₀ of ~0.0001) and cultured overnight (preculture). The low densities were used to ensure that the cells were growing exponentially the next morning. These cells were then diluted (20–50 times) and subcultured in prewarmed fresh glucose minimal medium (experimental culture). The cells grew exponentially

for at least 4 more doublings before they were spun down and resuspended in the same type of minimal medium without glucose (i.e., starvation medium). On the third day of the starvation, a small volume of the culture was transferred to fresh prewarmed LB medium containing ampicillin (BioBasic) for the CFU assays or microscope experiments. See *SI Appendix, Supplementary Method* for the details of the CFU assays.

Microscopy. All our single-cell-level observations were made using an inverted microscope (Olympus IX83). The microscope had an automated mechanical XY stage and autofocus, which were controlled by MetaMorph software (Molecular Devices). The microscope is housed in an incubator (InVivo Scientific), which ensured maintenance of a desired temperature in the experiments (37 °C). Images were captured using a Neo 5.5 sCMOS camera (Andor). Image analysis was performed using MicroBJ, a freely available plug-in for the ImageJ software (71). See *SI Appendix, Supplementary Method* for the details of the microscope experiments.

ACKNOWLEDGMENTS. This work was supported by Research Corporation for Science Advancement (24097) and the Human Frontier Science Program (RGY0072/2015).

1. A. Nicholson, Y.-D. Wong, Are accidents Poisson distributed? A statistical test. *Accid. Anal. Prev.* **25**, 91–97 (1993).
2. S. P. Huestis, Understanding the origin and meaning of the radioactive decay equation. *J. Geosci. Educ.* **50**, 524–527 (2002).
3. M. B. Elowitz, A. J. Levine, E. D. Siggia, P. S. Swain, Stochastic gene expression in a single cell. *Science* **297**, 1183–1186 (2002).
4. M. Thattai, A. van Oudenaarden, Intrinsic noise in gene regulatory networks. *Proc. Natl. Acad. Sci. U.S.A.* **98**, 8614–8619 (2001).
5. D. L. Jones, R. C. Brewster, R. Phillips, Promoter architecture dictates cell-to-cell variability in gene expression. *Science* **346**, 1533–1536 (2014).
6. A. Sigal *et al.*, Variability and memory of protein levels in human cells. *Nature* **444**, 643–646 (2006).
7. L. A. Sepúlveda, H. Xu, J. Zhang, M. Wang, I. Golding, Measurement of gene regulation in individual cells reveals rapid switching between promoter states. *Science* **351**, 1218–1222 (2016).
8. D. W. Austin *et al.*, Gene network shaping of inherent noise spectra. *Nature* **439**, 608–611 (2006).
9. Y. Taniguchi *et al.*, Quantifying *E. coli* proteome and transcriptome with single-molecule sensitivity in single cells. *Science* **329**, 533–538 (2010).
10. H. Maamar, A. Raj, D. Dubnau, Noise in gene expression determines cell fate in *Bacillus subtilis*. *Science* **317**, 526–529 (2007).
11. P. J. Choi, L. Cai, K. Frieda, X. S. Xie, A stochastic single-molecule event triggers phenotype switching of a bacterial cell. *Science* **322**, 442–446 (2008).
12. G. M. Süel, R. P. Kulkarni, J. Dworkin, J. Garcia-Ojalvo, M. B. Elowitz, Tunability and noise dependence in differentiation dynamics. *Science* **315**, 1716–1719 (2007).
13. G. Balázs, A. van Oudenaarden, J. J. Collins, Cellular decision making and biological noise: From microbes to mammals. *Cell* **144**, 910–925 (2011).
14. M. Ackermann, A functional perspective on phenotypic heterogeneity in microorganisms. *Nat. Rev. Microbiol.* **13**, 497–508 (2015).
15. A. Brauner, N. Shores, O. Fridman, N. Q. Balaban, An experimental framework for quantifying bacterial tolerance. *Biophys. J.* **112**, 2664–2671 (2017).
16. K. Lewis, Persister cells. *Annu. Rev. Microbiol.* **64**, 357–372 (2010).
17. K. Gerdes, E. Maisonneuve, Bacterial persistence and toxin-antitoxin loci. *Annu. Rev. Microbiol.* **66**, 103–123 (2012).
18. J. Bigger, Treatment of staphylococcal infections with penicillin by intermittent sterilisation. *Lancet* **244**, 497–500 (1944).
19. Y. Shan, D. Lazinski, S. Rowe, A. Camilli, K. Lewis, Genetic basis of persister tolerance to aminoglycosides in *Escherichia coli*. *MBio* **6**, e00078-15 (2015).
20. D. O. Osbourne, V. W. C. Soo, I. Konieczny, T. K. Wood, Polyphosphate, cyclic AMP, guanosine tetraphosphate, and c-di-GMP reduce in vitro Lon activity. *Bioengineered* **5**, 264–268 (2014).
21. B. C. M. Ramisetty, D. Ghosh, M. Roy Chowdhury, R. S. Santhosh, What is the link between stringent response, endoribonuclease encoding type II toxin-antitoxin systems and persistence? *Front. Microbiol.* **7**, 1882 (2016).
22. J.-S. Kim, T. K. Wood, Tolerant, growing cells from nutrient shifts are not persister cells. *MBio* **8**, e00354-17 (2017).
23. A. Harms, C. Fino, M. A. Sørensen, S. Semsey, K. Gerdes, Prophages and growth dynamics confound experimental results with antibiotic-tolerant persister cells. *MBio* **8**, e01964-17 (2017).
24. M. A. Orman, M. P. Brynildsen, Dormancy is not necessary or sufficient for bacterial persistence. *Antimicrob. Agents Chemother.* **57**, 3230–3239 (2013).
25. N. Q. Balaban, J. Merrin, R. Chait, L. Kowalik, S. Leibler, Bacterial persistence as a phenotypic switch. *Science* **305**, 1622–1625 (2004).
26. P. Patra, S. Klumpp, Population dynamics of bacterial persistence. *PLoS One* **8**, e62814 (2013).
27. B. R. Levin, K. I. Udekwu, Population dynamics of antibiotic treatment: A mathematical model and hypotheses for time-kill and continuous-culture experiments. *Antimicrob. Agents Chemother.* **54**, 3414–3426 (2010).
28. G. Carvalho, C. Guilhen, D. Balestrino, C. Forestier, J.-D. Mathias, Relating switching rates between normal and persister cells to substrate and antibiotic concentrations: A mathematical modelling approach supported by experiments. *Microb. Biotechnol.* **10**, 1616–1627 (2017).
29. R. J. Allen, B. Waclaw, Bacterial growth: A statistical physicist's guide. *Rep. Prog. Phys.* **82**, 016601 (2019).
30. D. Shah *et al.*, Persisters: A distinct physiological state of *E. coli*. *BMC Microbiol.* **6**, 53 (2006).
31. A. Jöers, T. Tenson, Growth resumption from stationary phase reveals memory in *Escherichia coli* cultures. *Sci. Rep.* **6**, 24055 (2016).
32. C. Vulin, N. Leimer, M. Huemer, M. Ackermann, A. S. Zinkernagel, Prolonged bacterial lag time results in small colony variants that represent a sub-population of persisters. *Nat. Commun.* **9**, 4074 (2018).
33. I. Levin-Reisman *et al.*, Automated imaging with ScanLag reveals previously undetectable bacterial growth phenotypes. *Nat. Methods* **7**, 737–739 (2010).
34. H. Luidalepp, A. Jöers, N. Kaldalu, T. Tenson, Age of inoculum strongly influences persister frequency and can mask effects of mutations implicated in altered persistence. *J. Bacteriol.* **193**, 3598–3605 (2011).
35. M. A. Orman, M. P. Brynildsen, Inhibition of stationary phase respiration impairs persister formation in *E. coli*. *Nat. Commun.* **6**, 7983 (2015).
36. G. Carret, J. P. Flandrois, J. R. Lobry, Biphasic kinetics of bacterial killing by quinolones. *J. Antimicrob. Chemother.* **27**, 319–327 (1991).
37. I. Keren, N. Kaldalu, A. Spoering, Y. Wang, K. Lewis, Persister cells and tolerance to antimicrobials. *FEMS Microbiol. Lett.* **230**, 13–18 (2004).
38. R. Allen, B. Waclaw, Antibiotic resistance: A physicist's view. *Phys. Biol.* **13**, 045001 (2016).
39. M. Newman, Power laws, Pareto distributions and Zipf's law. *Contemp. Phys.* **46**, 323–351 (2005).
40. L. Boulos, M. Prévost, B. Barbeau, J. Coallier, R. Desjardins, LIVE/DEAD BacLight : Application of a new rapid staining method for direct enumeration of viable and total bacteria in drinking water. *J. Microbiol. Methods* **37**, 77–86 (1999).
41. R. López-Amorós, J. Comas, J. Vives-Rego, Flow cytometric assessment of *Escherichia coli* and *Salmonella typhimurium* starvation-survival in seawater using rhodamine 123, propidium iodide, and oxonol. *Appl. Environ. Microbiol.* **61**, 2521–2526 (1995).
42. J. Comas, J. Vives-Rego, Assessment of the effects of gramicidin, formaldehyde, and surfactants on *Escherichia coli* by flow cytometry using nucleic acid and membrane potential dyes. *Cytometry* **29**, 58–64 (1997).
43. H. Sträuber, S. Müller, Viability states of bacteria—specific mechanisms of selected probes. *Cytometry A* **77**, 623–634 (2010).
44. E. Şimşek, M. Kim, The emergence of metabolic heterogeneity and diverse growth responses in isogenic bacterial cells. *ISME J.* **12**, 1199–1209 (2018).
45. Z. Yao, D. Kahne, R. Kishony, Distinct single-cell morphological dynamics under beta-lactam antibiotics. *Mol. Cell* **48**, 705–712 (2012).
46. E. Maisonneuve, K. Gerdes, Molecular mechanisms underlying bacterial persisters. *Cell* **157**, 539–548 (2014).
47. R. Trastoy *et al.*, Mechanisms of bacterial tolerance and persistence in the gastrointestinal and respiratory environments. *Clin. Microbiol. Rev.* **31**, e00023-18 (2018).
48. H. S. Moyed, K. P. Bertrand, hipA, a newly recognized gene of *Escherichia coli* K-12 that affects frequency of persistence after inhibition of murein synthesis. *J. Bacteriol.* **155**, 768–775 (1983).
49. T. Dörr, M. Vulić, K. Lewis, Ciprofloxacin causes persister formation by inducing the TisB toxin in *Escherichia coli*. *PLoS Biol.* **8**, e1000317 (2010).
50. N. Vázquez-Laslop, H. Lee, A. A. Neyfakh, Increased persistence in *Escherichia coli* caused by controlled expression of toxins or other unrelated proteins. *J. Bacteriol.* **188**, 3494–3497 (2006).
51. Y. Kim, T. K. Wood, Toxins Hha and CspD and small RNA regulator Hfq are involved in persister cell formation through MqsR in *Escherichia coli*. *Biochem. Biophys. Res. Commun.* **391**, 209–213 (2010).

52. Y. Pu *et al.*, Enhanced efflux activity facilitates drug tolerance in dormant bacterial cells. *Mol. Cell* **62**, 284–294 (2016).
53. Y. Li, Y. Zhang, PhoU is a persistence switch involved in persister formation and tolerance to multiple antibiotics and stresses in *Escherichia coli*. *Antimicrob. Agents Chemother.* **51**, 2092–2099 (2007).
54. N. M. Vega, K. R. Allison, A. S. Khalil, J. J. Collins, Signaling-mediated bacterial persister formation. *Nat. Chem. Biol.* **8**, 431–433 (2012).
55. N. Wu *et al.*, Ranking of persister genes in the same *Escherichia coli* genetic background demonstrates varying importance of individual persister genes in tolerance to different antibiotics. *Front. Microbiol.* **6**, 1003 (2015).
56. T. Dörr, K. Lewis, M. Vulić, SOS response induces persistence to fluoroquinolones in *Escherichia coli*. *PLoS Genet.* **5**, e1000760 (2009).
57. E. A. Debbia, S. Roveta, A. M. Schito, L. Gualco, A. Marchese, Antibiotic persistence: The role of spontaneous DNA repair response. *Microb. Drug Resist.* **7**, 335–342 (2001).
58. S. Hansen, K. Lewis, M. Vulić, Role of global regulators and nucleotide metabolism in antibiotic tolerance in *Escherichia coli*. *Antimicrob. Agents Chemother.* **52**, 2718–2726 (2008).
59. C. Miller *et al.*, SOS response induction by β -lactams and bacterial defense against antibiotic lethality. *Science* **305**, 1629–1631 (2004).
60. P. J. Johnson, B. R. Levin, Pharmacodynamics, population dynamics, and the evolution of persistence in *Staphylococcus aureus*. *PLoS Genet.* **9**, e1003123 (2013).
61. J. C. J. Ray *et al.*, Cellular growth arrest and persistence from enzyme saturation. *PLoS Comput. Biol.* **12**, e1004825 (2016).
62. S. M. Amato *et al.*, The role of metabolism in bacterial persistence. *Front. Microbiol.* **5**, 70 (2014).
63. K. R. Allison, M. P. Brynildsen, J. J. Collins, Heterogeneous bacterial persisters and engineering approaches to eliminate them. *Curr. Opin. Microbiol.* **14**, 593–598 (2011).
64. K. R. Allison, M. P. Brynildsen, J. J. Collins, Metabolite-enabled eradication of bacterial persisters by aminoglycosides. *Nature* **473**, 216–220 (2011).
65. V. Defraigne, M. Fauvart, J. Michiels, Fighting bacterial persistence: Current and emerging anti-persister strategies and therapeutics. *Drug Resist. Updat.* **38**, 12–26 (2018).
66. F. M. Vallette *et al.*, Dormant, quiescent, tolerant and persister cells: Four synonyms for the same target in cancer. *Biochem. Pharmacol.* **162**, 169–176 (2019).
67. J. Wuyts, P. Van Dijck, M. Holtappels, Fungal persister cells: The basis for recalcitrant infections? *PLoS Pathog.* **14**, e1007301 (2018).
68. K. S. Farquhar *et al.*, Role of network-mediated stochasticity in mammalian drug resistance. *Nat. Commun.* **10**, 2766 (2019).
69. M. Kim *et al.*, Need-based activation of ammonium uptake in *Escherichia coli*. *Mol. Syst. Biol.* **8**, 616 (2012).
70. L. N. Csonka, T. P. Ikeda, S. A. Fletcher, S. Kustu, The accumulation of glutamate is necessary for optimal growth of *Salmonella typhimurium* in media of high osmolality but not induction of the proU operon. *J. Bacteriol.* **176**, 6324–6333 (1994).
71. A. Ducret, E. M. Quardokus, Y. V. Brun, MicroBJ, a tool for high throughput bacterial cell detection and quantitative analysis. *Nat. Microbiol.* **1**, 16077 (2016).